Consecutive and Parallel Dissociation of Energy-Selected $Co(CO)_3NO^+$ Ions

Bálint Sztáray† and Tomas Baer*

Department of Chemistry, University of North Carolina, Chapel Hill, North Carolina 27599-3290

Received: April 3, 2002; In Final Form: June 19, 2002

Photoelectron photoion coincidence (PEPICO) spectroscopy has been used to investigate the dissociation dynamics of the cobalt tricarbonyl nitrosyl ion, $Co(CO)_3NO^+$. The ionization energy of $Co(CO)_3NO$ was measured from the threshold photoelectron spectrum to be 8.33 ± 0.04 eV. The dissociation of the molecular ion proceeds by two sequential carbonyl-loss steps and then a parallel carbonyl- or nitrosyl-loss step. The first two reactions were observed to be slow (lifetimes in the microsecond range). By simulating the resulting asymmetric time-of-flight peak shapes and the relative ion abundances (breakdown curves), 0 K onsets for the following fragment ions were determined: $Co(CO)_2NO^+$, 9.28 ± 0.02 eV; $CoCONO^+$, 10.43 ± 0.02 eV; $CoNO^+$, 12.00 ± 0.02 eV; $CoCO^+$, 12.07 ± 0.02 eV. Combining these onsets with the experimental adiabatic ionization energy of $Co(CO)_3NO^+$, the three cobalt−carbonyl bond energies in $Co(CO)_xNO^+$ ($x = 1-3$) were determined along with the cobalt-nitrosyl bond energy in $CoCONO^+$. Using a literature value for the $[Co-CO]^+$ bond energy, the 0 K heats of formation of the above-mentioned molecular and fragment ions and of the neutral compound, $Co(CO)_3NO$, were determined. Using these thermochemical data, the cobalt−nitrosyl bond energies were also derived for $Co(CO)_3NO^+$ and $CoNO^+$. The latter is in good agreement with a theoretical literature value, while the first one explains why there is no observable NO loss from the molecular ion, $Co(CO)_3NO^+$. Room-temperature values of the heats of formation are also given using the calculated harmonic frequencies.

Introduction

Transition metal complexes are widely used today as catalysts or chemical vapor deposition (CVD) precursors. An especially interesting and useful group of complexes is the transition metal carbonyls. In these compounds, the usual starting step for the formation of the catalytically active, coordinatively unsaturated species is the metal−carbonyl bond rupture. Similarly, in metal−organic CVD (MOCVD) processes at elevated temperatures, the first-leaving group is usually the carbonyl. Therefore, the thermochemistry, and especially the transition metal carbonyl bond energies are vitally important. In the past few years, we have investigated the neutral and ionic gas phase thermochemistry of a number of organometallic complexes, such as $CpCo(CO)_2$,[1,2] $CpMn(CO)_3$,[3] $BzCr(CO)_3$,[4] CpMnCp,[5] and BzCrBz[6] ($Cp = C_5H_5$, $Bz = C_6H_6$).

Cobalt tricarbonyl nitrosyl has numerous uses in both homogeneous and heterogeneous catalysis, chemical vapor deposition, and more recently in nanotechnology. For example, $Co(CO)_3NO$ was used for producing phenylacetic acid and its derivatives by catalytic carbonylation[7] and for the catalytic alkylation of allylic substrates.[8] It is also widely used in constructing heterogeneous catalysts with chemical vapor deposition on zeolites. These catalysts were used for hydrodesulfurization[9,10] as well as for CO hydrogenation.[11] Cobalt tricarbonyl nitrosyl was also used as the precursor in chemical vapor deposition experiments to synthesize cobalt,[12,13] cobalt−copper alloy,[14] cobalt silicide,[15,16] and cobalt oxinitride[17] thin films or cobalt-doped semiinsulating layers.[18,19] Recently, $Co(CO)_3NO$ was used as a precursor in nanotechnology for producing cobalt filled carbon nanotubes[20,21] and nanoflasks.[22]

Numerous mass spectrometric studies have focused on $Co(CO)_3NO$. The early experiments of Pignataro and co-workers with electron ionization reported an ionization potential of 8.75 eV.[23] The observed fragmentation pattern, which included all possible ions from $Co(CO)_3NO^+$ to the cobalt cation, Co^+, was explained in terms of a mechanism that allowed loss of NO and CO with equal probability from all intermediate $Co(CO)_nNO_m^+$ ions. Such a mechanism leads to the $CoCO^+$ ion via three equally probably paths compared to just one path for $CoNO^+$ production, thereby accounting for the higher peak intensity of $CoCO^+$. In a later publication, the appearance energy of the $Co(CO)_2NO^+$ fragment ion was determined to be 9.65 eV.[24]

The first photoionization (PI) and photoelectron (PE) spectra for $Co(CO)_3NO$ were carried out by Lloyd and Schlag,[25] who reported adiabatic and vertical ionization energies of 8.11 ± 0.03 and 9.05 ± 0.17 eV, respectively. A later He(I) PES of $Co(CO)_3NO$ published by Hiller et al.[26] found these values to be 8.26 ± 0.03 and 8.90 ± 0.02 eV, respectively. The quoted errors for the adiabatic ionization energies in both of these studies are probably too small because of the well-known difficulties in identifying an onset in a signal that rises slowly out of the background.

High energy photoelectron spectra (XPS) of $Co(CO)_3NO$ were taken by Barber and co-workers,[27] as well as by Chen and Jolly.[28] The analysis of the binding-energy shifts indicates a larger back-bonding in the case of the nitrosyl ligands than of the carbonyls. These results confirm the common findings that the nitrosyl ligands bond more strongly to the metal center than the carbonyls.

In this study we investigate the gas-phase dissociation kinetics of energy-selected $Co(CO)_3NO^+$ ions using threshold photoelectron photoion coincidence (TPEPICO) spectroscopy. The experimental results, with a statistical analysis of the dissociation rates and the energy partitioning in the dissociation steps, provide bond energies and heats of formation of both the

* Corresponding author.
† On leave from the Eötvös Loránd University, Budapest, Hungary.

10.1021/jp020897h CCC: $22.00
Published on Web 08/09/2002

molecular and various fragment ions and of the neutral cobalt tricarbonyl nitrosyl. Using a literature value[29] for the heat of formation of $Co(CO)_3^+$, another cobalt−nitrosyl bond energy—a rupture of which does not appear in the experiment—can be obtained.

Experimental Approach

Cobalt tricarbonyl nitrosyl was purchased from Strem Chemicals and was used without further purification. Because of the sufficiently high vapor pressure of the sample, it was introduced through a room temperature needle to the ionization region of the spectrometer. The details of the threshold photoelectron photoion coincidence (TPEPICO) spectrometer has been described previously.[30,31] Briefly, the room-temperature sample molecules were ionized with vacuum ultraviolet (VUV) light from a H_2 discharge lamp dispersed by a 1 m normal incidence vacuum monochromator. The VUV wavelengths were calibrated using the hydrogen Lyman-α resonance line. The ions and the electrons were extracted in opposite directions with an electric field of 20 V/cm. Threshold photoelectrons were selected by a steradiancy analyzer that consists of a flight tube with small apertures to stop energetic electrons. Further selection of the threshold photoelectrons was provided by a hemispherical electrostatic sector analyzer resulting in a ∼35 meV combined photon and electron resolution. After exiting the 5 cm long first acceleration region, the ions entered a second (0.5 cm long) acceleration region in which they were accelerated to 210 eV. After traversing a 32 cm field-free drift tube, they were detected with a Chevron alignment multichannel plate (MCP) detector. The electrons were detected with a Channeltron electron multiplier. The electron and ion signals served as start and stop pulses for measuring the ion time-of-flight (TOF), and the TOF for each coincidence event was stored on a multichannel pulse height analyzer. TOF distributions were obtained in 1−48 h depending on the signal intensity and the desired spectrum quality.

The PEPICO spectra were used for two purposes. First, the fractional abundances of the parent and the daughter ions were measured as a function of the photon energy (breakdown curve). Second, ion decay rates were extracted from asymmetric TOF distributions of the daughter ion signal. This asymmetry is the result of slowly dissociating (metastable) ions dissociating in the 5 cm acceleration region, resulting in a time-of-flight between the parent and the daughter ion's flight time. These two types of information were used together in the data analysis as described in a later section in detail.

Quantum Chemical Calculations

For the calculation of the internal energy distribution of the neutral cobalt tricarbonyl nitrosyl, and also for the RRKM rate constant calculations, harmonic vibrational frequencies were needed of neutral $Co(CO)_3NO$, of the molecular and fragment ions, and of the four transition states. Because, as it is discussed later, the lowest few frequencies of the transition states were scaled to fit to the experimental dissociation rates, the accuracy of the individual frequencies were not a real concern. Thus, we have used only one level of theory with one—sufficiently large—basis set. All the calculations were carried out at the DFT level using B3LYP functional[32] and 6-311G** basis set.[33] Various spin states were calculated for the neutral and ionic species and the most stable were used to calculate the vibrational frequencies. The neutral molecule was determined to be a singlet, while the nitrosyl-containing ions were found to be doublets. In the case of $CoCO^+$, the triplet state was found to be more stable than the singlet. All neutral and equilibrium ion structures were optimized in redundant internal coordinates using Pulay's force method.[34] Because these dissociations proceed with no reverse barrier, the transition states do not correspond to a critical point on the potential energy surface. To approximate the structure and vibrational frequencies of the transition states, the metal−carbonyl bond distances of the leaving carbonyl groups were fixed at 4.0 Å and the energy optimized with respect to the remaining coordinates. The distance of 4.0 Å was suggested by previous variational transition state theory (VTST) calculations of another cobalt−carbonyl complex.[1] All of the quantum-chemical calculations were carried out with the Gaussian98, revision A.7,[35] program. In the RRKM-calculations of the dissociation rates, the TS frequencies were used as the starting point for fitting the experimental dissociation rate curves. The lowest four frequencies of the transition states, which turn into product rotations, were scaled in order to fit the calculated TOF distributions and breakdown diagrams to the experimentally measured data. These harmonic vibrational frequencies are listed in Table 1.

Experimental Results

A scan of the total ion and threshold electron signals were used to extract the adiabatic ionization energy of 8.33 eV. This value is slightly higher than those quoted by Lloyd and Schlag[25] and Hillier et al.[26] who reported 8.11 and 8.26 eV, respectively. The determination of the adiabatic ionization energy is quite difficult unless vibrational resolved and assigned PES peaks are available. This is rarely the case for polyatomic molecules. Thus, the adiabatic ionization energy has a larger uncertainty than the vertical ionization energy, which is simply the first peak position of the PES spectrum.

TOF mass spectra of $Co(CO)_3NO$ were collected in the photon energy range of 9−13.5 eV. Typical time-of-flight distributions are shown in Figure 1a-c for all three dissociation steps. The experimental data are plotted as dots while the solid lines show the fitted TOF distributions as discussed in the data analysis section. Below a photon energy of 10 eV, the two peaks correspond to the molecular ion, $Co(CO)_3NO^+$ at 30.3μs, and its daughter ion, $Co(CO)_2NO^+$ at 27.7 μs. At photon energies between 10 and 12 eV, the two peaks are due to $Co(CO)_2NO^+$ and its dissociation product, $CoCONO^+$. Finally, near the upper limit of our light source, at photon energies in excess of 12.5 eV, we observe only $CoCONO^+$ ions and its two dissociation products, $CoNO^+$ and $CoCO^+$. It is interesting that at 12.533 eV the majority of the daughter ions are $CoNO^+$, while at 13.116 eV, the dominant peak has shifted markedly toward the lower mass $CoCO^+$ ion. Because the maximum available photon energy in the instrument is about 13.5 eV, no bare cobalt ion was observed.

As shown in Figure 1a and 1b, the daughter ion TOF distributions are asymmetric at energies close to their respective appearance energies. This indicates that the ions dissociate while travelling in the first acceleration region of the ion optics. If an ion dissociates in this region, its final velocity as it enters the drift region will be larger than that of the parent ion, but less than that of a rapidly produced daughter ion. Thus, the total flight time of these slowly produced ions falls between that of the parent ion and that of the rapidly produced daughter ion. Since there is a distribution of lifetimes at a given dissociation rate, a quasi-exponential shape of the time-of-flight peak is observed. The decay rate can be extracted from the analysis of the peak shapes. The ions that dissociate after the acceleration region are detected as parent ions. In the case of slow reactions,

TABLE 1: Harmonic Vibrational Frequencies (in cm^{-1}) Used in the Density of States and Number of States Calculations[a]

$Co(CO)_3NO$	$Co(CO)_3NO^+$	$[Co(CO)_2NO\cdots CO]^+$	$Co(CO)_2NO^+$	$[CoCONO\cdots CO]^+$	$CoCONO^+$	$[CoNO\cdots CO]^+$	$[CoCO\cdots NO]^+$
61.1	29.0	25.0[b]	51.1	8.0[b]	32.2	15.0[b]	8.0[b]
61.1	57.8	29.0[b]	66.4	15.0[b]	201.6	29.0[b]	11.0[b]
77.1	66.0	32.0[b]	69.7	44.0[b]	204.7	30.0[b]	12.0[b]
77.1	71.2	119.0[b]	176.4	148.0[b]	246.2	93.0[b]	19.0[b]
86.7	78.4	69.4	225.7	125.7	246.6	246.6	226.6
261.2	202.7	88.4	240.8	220.8	293.4	450.0	439.9
261.2	223.7	89.5	269.2	239.2	539.9	1978.7	1950.0
288.7	234.9	191.8	301.1	312.5	1938.7	2297.7	2250.0
411.5	277.9	229.4	312.5	360.2	2197.7		
444.7	295.9	249.2	360.2	368.2			
444.7	319.0	311.2	368.2	459.9			
462.1	343.1	337.3	459.9	1880.0			
478.1	359.3	376.3	1868.0	2145.0			
478.1	362.4	424.4	2130.7	2165.0			
566.7	403.4	448.0	2158.3				
566.7	418.6	450.9					
631.7	446.9	1911.2					
1829.4	1904.3	2132.3					
2006.0	2124.3	2141.4					
2006.0	2133.2	2157.1					
2067.7	2155.9						

[a] Imaginary frequencies of the transition states are not listed. [b] Frequencies fitted to the experimental data.

the relatively short time scale of the PEPICO experiment leads to the so-called kinetic shift[36] as discussed in an earlier paper in detail.[1]

Figure 2 shows the breakdown diagram of the dissociation of $Co(CO)_3NO^+$. The fractional abundances of the molecular ion and the fragment ions are plotted as a function of the photon energy. The points are the experimentally determined ratios with error estimates while the solid lines show the results of the RRKM simulations. For the first two dissociations, the abundance of the ions was readily available from the TOF distributions. However, the TOF peaks of the last two daughter ions, $CoCO^+$ and $CoNO^+$, overlap, and the two peaks were deconvoluted by representing each peak by a Gaussian function. One of the most interesting features of this plot is the slope of the breakdown curves at the crossover points. In the case of the first dissociation, $Co(CO)_3NO^+ \rightarrow Co(CO)_2NO^+ + CO$, the breakdown of the parent ion abundance is quite steep indicating a narrow distribution of the ion internal energy. The second crossover corresponding to the carbonyl loss from $Co(CO)_2NO^+$ is much wider. The slope of the breakdown curves at the third consecutive step, the parallel dissociation of $CoCONO^+$ into $CoCO^+$ and $CoNO^+$ is even flatter indicating a wide distribution of the ion internal energies. These results will be discussed in the Data Analysis section in more detail as we made significant efforts to properly model this behavior.

Data Analysis

The reaction mechanism for the $Co(CO)_3NO^+$ ions with increasing internal energy involves the sequential loss of two carbonyl groups and a parallel step of losing a carbonyl or a nitrosyl group. The extraction of thermochemical data and bond

$$Co(CO)_3NO^+ \rightarrow \underset{+\,CO}{Co(CO)_2NO^+} \rightarrow \underset{+\,CO}{CoCONO^+} \begin{cases} \longrightarrow CoCO^+ + NO \\ \searrow\ CoNO^+ + CO \end{cases} \quad (1)$$

energies from the experimental results requires a detailed analysis of dissociation rates in terms of the ion energy distribution. Although the TPEPICO resolution used in this study is about 35 meV, the thermal energy distribution of the molecular ion, $Co(CO)_3NO^+$, is much wider. To properly model the three consecutive reactions, it is necessary to interpret the measured reaction rates in terms of a distribution of $k(E)$ in which the energy (E) extends over this thermal energy distribution. Thus, the first step is the calculation of the thermal energy distribution of the neutral cobalt-tricarbonyl-nitrosyl using the following formula:

$$P(E) = \frac{\rho(E)e^{-E/RT}}{\int_0^\infty \rho(E)e^{-E/RT}} \quad (2)$$

in which $\rho(E)$ is the rovibrational density of states calculated using a direct count method.[37,38] The harmonic frequencies, shown in Table 1, were calculated using density functional theory with the B3LYP functional and 6-311G** basis set, and then scaled with a factor of 0.95. The rotational density of states of the molecule was calculated as a symmetrical top using the rotational constants 1.131 GHz and 2 × 1.076 GHz provided by the B3LYP/6-311G** optimized structure. The thermal energy distribution of the neutral $Co(CO)_3NO$ was used to obtain the internal energy distribution of the parent ion, $Co(CO)_3NO^+$. This latter function can be calculated by convoluting the neutral's thermal energy distribution with the electron energy analyzer function and adding the difference of the photon energy and the adiabatic ionization energy. An example of the internal energy distribution of the molecular ion is shown on the right side of Figure 3 or 4. The analyzer function can be measured from a threshold photoelectron spectrum of a noble or a diatomic gas, such as Xe or NO.

The energy distribution of the daughter ions, $Co(CO)_2NO^+$ and $CoCONO^+$, is somewhat more complicated to determine. After $Co(CO)_3NO^+$ ions of a particular energy, E, dissociate, they leave behind $Co(CO)_2NO^+ + CO$ products in a distribution of internal energies from 0 to $E - E_o$. One way to calculate the product energy distribution is to employ the Klots equation:[38,39]

$$E - E_0 = E_{tr} + E_{ro}(CO) + E_v(CO) + E_{ro}(Co(CO)_2NO^+) + E_v(Co(CO)_2NO^+)$$

$$= kT^* + kT^* + 0 + \frac{3}{2}kT^* + \sum_{i=1}^{s} \frac{h\nu}{e^{h\nu_i/kT^*} - 1} \quad (3)$$

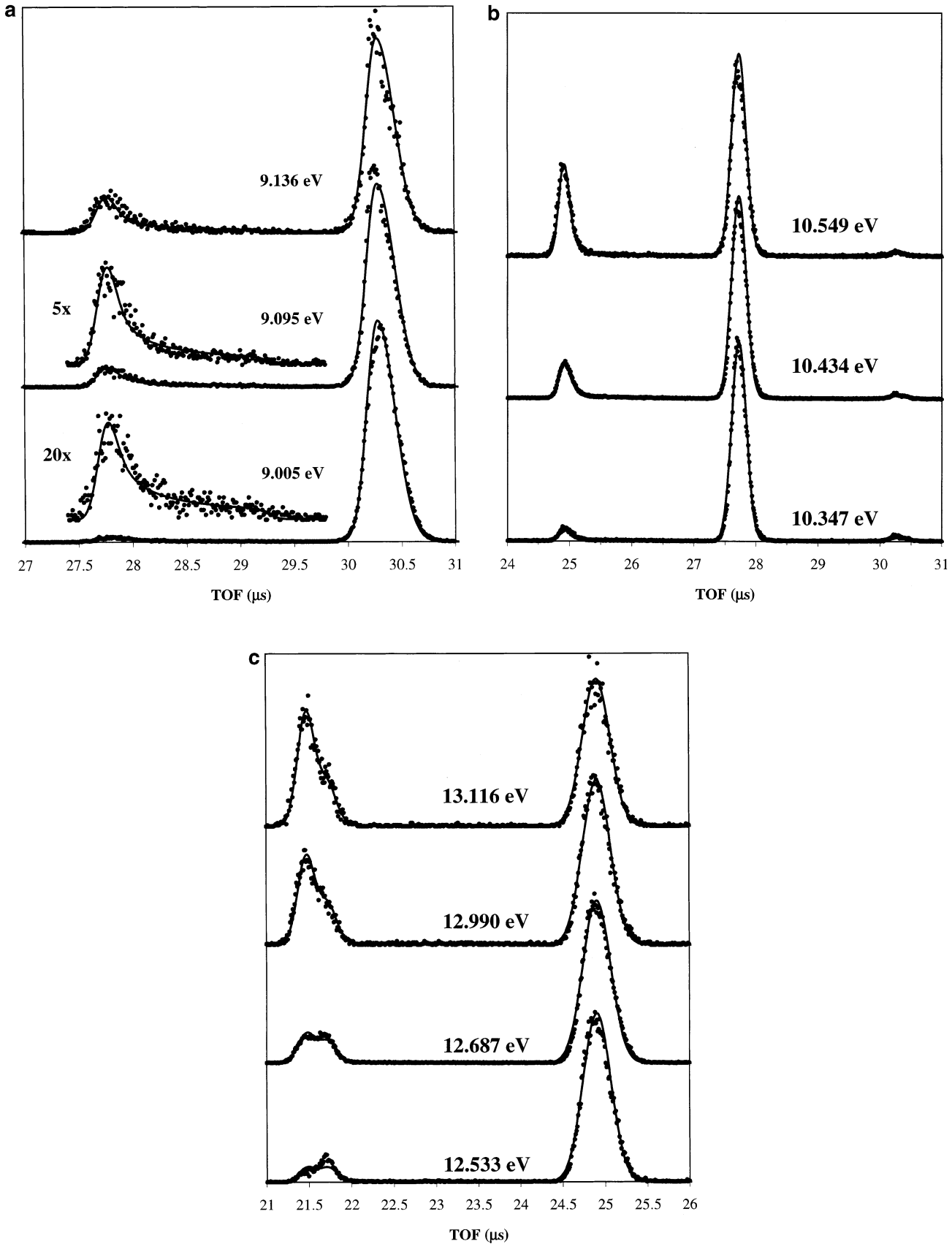

Figure 1. Ion TOF distributions at selected photon energies. Points are the experimental data, while the solid lines show the calculated TOF distributions as described in the text. (a) The first carbonyl loss: the asymmetric peak between 27.5 and 29.5 μs is assigned to the $Co(CO)_2NO^+$ ion, while the symmetric peak at 30.3 μs belongs to the parent ion, $Co(CO)_3NO^+$. (b) The second carbonyl loss: the first peak at about 25 μs is due to the second daughter ion, $CoCONO^+$, while the second peak between 27.5 and 28 μs belongs to $Co(CO)_2NO^+$. Traces of the molecular ion, $Co(CO)_3NO^+$ are also visible above 30 μs. (c) The third carbonyl loss in parallel with NO loss from $CoCONO^+$: the first two peaks between 21 and 22 ms correspond to $CoCO^+$ and to $CoNO^+$, respectively. The right-hand side peak is due to $CoCONO^+$.

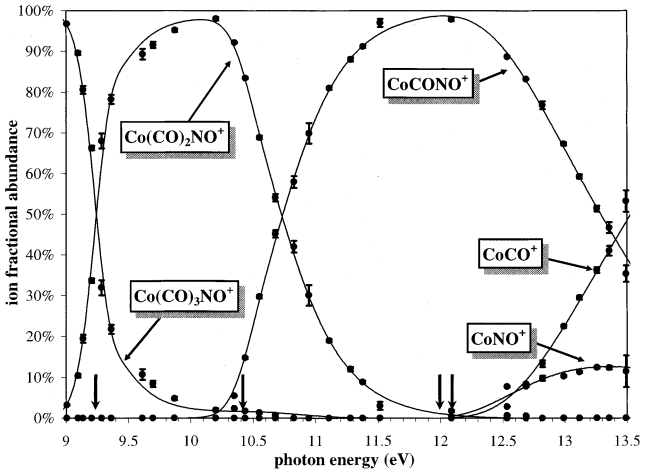

Figure 2. Breakdown curves of the three consecutive carbonyl-loss steps and the one parallel NO-loss step. The dots are the experimental data with error estimates. Solid lines indicate the results of the RRKM-simulation as described in the Data Analysis.

This equation assumes, in the spirit of the statistical theory, that the various modes of the dissociating system are in thermal equilibrium with each other. By solving this equation for the common temperature, T^*, the average rotational and vibrational energy remaining in the ionic fragment can be obtained. By carrying out the above procedure for each energy in the parent ion internal energy distribution, the energy distribution of the daughter ion can be obtained. This method was used and has been described in a number of our earlier papers.[1,3,4,5] However, it is not strictly correct because this approach assigns a fixed average internal energy to each product ion for each energy in the original energy distribution, rather than a distribution of internal energies from 0 to $E - E_o$. A more precise modeling of the product energy distribution involves a convolution of the microcanonical product energy distribution function for each E energy with the internal energy distribution of the parent ion.[38] The product energy distribution for each total excess energy, $E - E_0$, has the following form:

$$P(E_i,E-E_0) = \frac{\rho_{Co(CO)_2NO^+}(E_i)\int_0^{E-E_0-E_i}\rho_{CO}(x)\rho_{tr}(E-E_0-E_i-x)\,dx}{\int_0^{E-E_0}\rho_{Co(CO)_2NO^+}(y)\left(\int_0^{E-E_0-y}\rho_{CO}(x)\rho_{tr}(E-E_0-y-x)\,dx\right)dy} \quad (4)$$

where $P(E_i,E-E_0)$ is the probability of the daughter ion internal energy E_i for a total excess energy $E - E_0$, the three ρ's are the ro-vibrational density of states of the daughter ion, the ro-vibrational density of states of CO, and the density of states associated with the two-dimensional translations of the dissociating fragments, respectively. The denominator is the normalization integral. The integral in the numerator is equal to the combined density of states of the CO and translation, ρ_{CO+tr} (or alternatively, the sum of the ro-vibrational states of the CO molecule, N_{CO}). The simplified equation then becomes

$$p(E_i) = \frac{\rho_{Co(CO)_2NO^+}(E_i)\rho_{CO+tr}(E-E_0-E_i)}{\int_0^{E-E_0}\rho_{Co(CO)_2NO^+}(x)\rho_{CO+tr}(E-E_0-x)\,dx} \quad (5)$$

The initial parent ion internal energy distribution and the resulting $Co(CO)_2NO^+$ and CO distributions calculated with eq 5 are shown in Figure 3. The parent ion, $Co(CO)_3NO^+$, has a relatively sharp internal energy distribution due to the TPEPICO

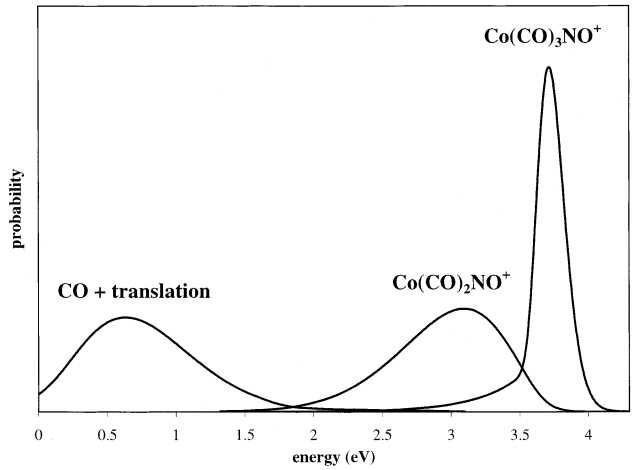

Figure 3. Partitioning of the excess internal energy of the molecular ion after a carbonyl loss. The majority of the excess energy remains in the ionic fragment, $Co(CO)_2NO^+$, while a significant amount is taken away by the leaving carbon monoxide molecule. Note the broadening of the internal energy distribution.

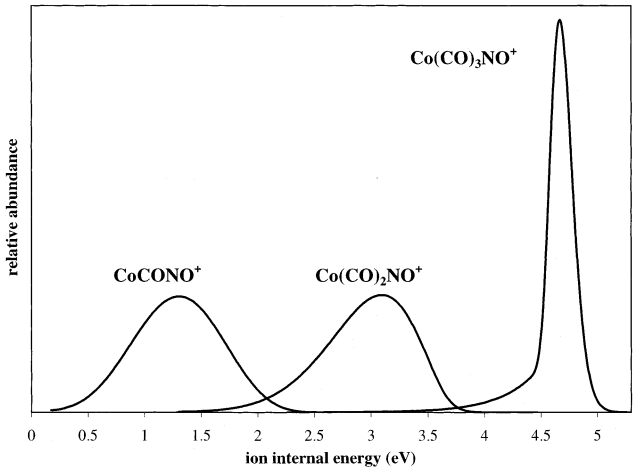

Figure 4. Internal energy distribution of the three parent ions, $Co(CO)_3NO^+$, $Co(CO)_2NO^+$ and $CoCONO^+$ at a photon energy of 12.8 eV. The internal energy distribution broadens as a result of the product energy distribution following each consecutive dissociation step.

energy selection. However, the daughter ion, $Co(CO)_2NO^+$, has a much broader internal energy distribution as the excess energy is distributed between the fragments after the dissociation. The internal energy distribution of the second daughter ion, $CoCONO^+$ can be calculated with the same method. As shown in Figure 4, this ion has an even broader energy distribution than $Co(CO)_2NO^+$, however, this increase is not as dramatic as it was in going from the parent ion to the first fragment.

Rate constants were calculated for the four unimolecular dissociation steps of the $Co(CO)_3NO^+$ ion. RRKM calculations were performed using the well-known formula[38,40]

$$k(E) = \frac{\sigma N^{\#}(E-E_0)}{h\rho(E)} \quad (6)$$

in which $N^{\#}(E - E_0)$ is the sum of states of the transition state from 0 to $E - E_0$ and $\rho(E)$ is the density of states of the ion measured from the bottom of the ion ground-state potential energy well. The symmetry parameter, σ is 3 in the first dissociation, 2 in the second, and 1 in the third two parallel steps. The ion vibrational frequencies used to calculate the density and sums of states in eq 6 are listed in Table 1.

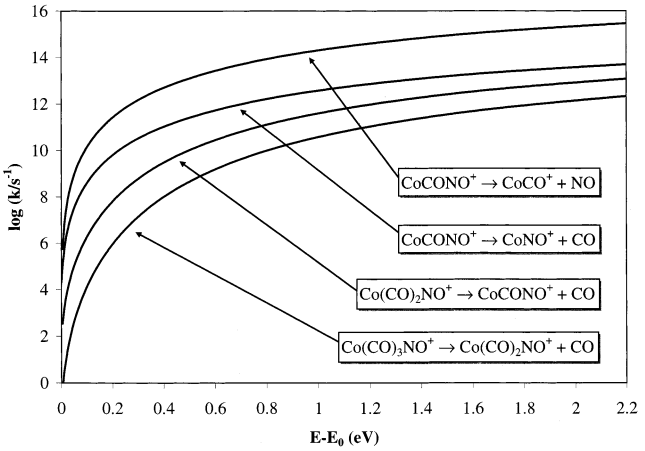

Figure 5. The RRKM calculated rate constants of the four dissociation reactions. The topmost curve corresponds to the nitrosyl-loss reaction with the highest activation barrier, but the fastest reaction rate. The lowest curve shows the slowest dissociation, the first carbonyl loss from the $Co(CO)_3NO^+$ molecular ion. The appearance of the asymmetric daughter ion TOF peaks is due to this slow reaction rate.

The ion TOF distribution and the breakdown diagram can be calculated using the following fixed information: the thermal energy distribution, the ionization energy, the ion TOF parameters (acceleration electric fields and the acceleration and drift distances), and the ion vibrational frequencies. The adiabatic ionization energy of 8.33 eV was obtained from TPES measurements with the same apparatus. The following variable parameters were adjusted until a best fit was obtained: the dissociation limits, the four lowest TS vibrational frequencies, which determine the entropy of activation, and to a limited extent the threshold electron analyzer function. The four lowest vibrational frequencies are ones that are converted from vibrations into overall product rotations. The calculations were carried out with a computer program using the simplex algorithm[41] for minimizing the following error function:

$$\text{error} = 1 - \frac{\langle E|S\rangle}{\sqrt{\langle E|E\rangle\langle S|S\rangle}} = 1 - \frac{\sum_i E_i S_i}{\sqrt{\sum_i E_i E_i \sum_i S_i S_i}} \quad (7)$$

where E_i and S_i are the experimental and simulated points for either the TOF distribution or the breakdown diagram. This error function varies from 1 to 0, the latter value corresponding to a perfect fit in which S and E are equal. This procedure has been described before in an earlier paper dealing with the dissociation of the cyclopentadienyl cobalt dicarbonyl ion, $CpCo(CO)_2^+$.[1]

The best fit to both the TOF distributions and the breakdown curves was obtained with the following parameters: barrier$_1$ = 0.95 eV, barrier$_2$ = 1.15 eV, barrier$_3$ = 1.57 eV, barrier$_4$ = 1.63 eV, and the lowest frequencies listed in Table 1. The first three energies are the three consecutive carbonyl loss reactions, while the fourth is the nitrosyl loss from $CoCONO^+$. The simulated breakdown curves and time-of-flight distributions are shown as solid curves in Figures 1 and 2. The RRKM rate constants are plotted in Figure 5. Using the fitted transition state frequencies, canonical activation entropies were also calculated. The four $\Delta S^{\#}$ values at 600 K are the following: 17.97, 28.20, 36.09, and 71.08 J/mol·K; while at 1000 K, 13.98, 24.12, 32.05, 67.17 J/mol·K. These numbers are characteristic of loose transition states.

The uncertainties in the derived parameters were studied by fixing the lowest four transition state frequencies at various values and carrying out the fitting procedure outlined above. This scheme simulates looser or tighter transition states, thereby altering the $k(E)$ rate curves. It was found that changing the lowest four frequencies by ±50% does not affect the simulated breakdown diagram significantly, but the quality of the TOF distributions get significantly worse. This is because the quasi-exponential shape of the asymmetric daughter ion distributions depends on the absolute dissociation rate, whereas the breakdown diagram depends only on the ratios of the rate constants. The optimized barrier heights change by ±20 meV with the altered transition state frequencies given above, which suggests an error bar of ±20 meV for these parameters.

The derived barriers correspond to dissociative photoionization limits of $Co(CO)_2NO^+$, $CoCONO^+$, $CoNO^+$, and $CoCO^+$ of 9.28 ± 0.02 eV, 10.43 ± 0.02 eV, 12.00 ± 0.02 eV, and 12.07 ± 0.02 eV, respectively. Previous $Co(CO)_2NO^+$ onset energies were reported by Pignataro and Lossing[24] (9.65 eV) on the basis of an energy-selected electron impact (EI) measurement, and by Lloyd and Schlag[25] (9.37 ± 0.10 eV) on the basis of an unspecified method of AE extraction from a total photoionization efficiency scan without benefit of mass analysis. The EI result probably suffered from the unfavorable threshold law of electron-impact ionization and neglect the kinetic shift due to the slow dissociation as discussed before in the case of $CpCo(CO)_2$. The close agreement between our result and the Lloyd-Schlag value is undoubtedly fortuitous. No other onsets for subsequent CO or NO loss steps have been reported.

Thermochemical Data

The heat of formation of $Co(CO)_3NO$ is not listed in any of the major thermochemical compilations,[42−44] One approach to obtaining this value using dissociative photoionization is to measure the energy required to dissociate the ion to $Co^+ + 3CO + NO$. Combining the measured onset with the known product heats of formation permits the determination of the neutral cobalt tricarbonyl nitrosyl heat of formation. Unfortunately, the photon energy range of our light source does not extend to sufficiently high energy to detect cobalt ions. However, the bond energy of $[Co-CO]^+$ has been determined in a number of experiments. Bowers and co-workers published product kinetic energy release distributions for reactions of Co^+ with acetone to eliminate CO, from which they derived a $[Co-CO]^+$ bond energy of 1.34 eV.[45] A reanalysis of these data, which require several assumptions about product energy partitioning, increased this value to 1.70 ± 0.13 eV (163.7 ± 12.6 kJ·mol^{-1}).[46] Armentrout and co-workers determined successive Co^+-CO bond energies in $CoCO_x+$ ions ($x = 1-5$) in collision induced dissociation (CID) experiments with Xe using guided-ion beam mass spectrometry.[29] Their value for the dissociation energy of $[Co-CO]^+$ is 1.80 ± 0.07 eV (173. 7 ± 6.8 kJ·mol^{-1}). Finally, a theoretical study by Barnes et al.[47] reported a $[Co-CO]^+$ bond energy of 1.62 eV using a size-consistent modified coupled pair functional method. The other final ionic product in our experiment is the cobalt nitrosyl ion, $CoNO^+$. However, no experimental bond energy is available. On the other hand, high-level ab initio calculation results were published by Thomas et al.[48] for the Co^+-NO bond energy. These results will be discussed later.

Using the zero Kelvin heats of formation from the NIST-JANAF thermochemical tables[49] of the Co^+ ion (1183.88 ± 1.0 kJ·mol^{-1}) and carbon monoxide (−113.81 ± 0.17 kJ·mol^{-1}) with the $[Co-CO]^+$ dissociation energy published by Armentrout,[29] we obtain a $CoCO^+$ 0 K heat of formation of 896 ± 7 kJ·mol^{-1}. By combining the $[CoCO\cdots NO]^+$ bond energy of

TABLE 2: Auxiliary and Derived Thermochemical Data (in kJ·mol^{-1})[a]

	D_0 (Co−CO)	D_0 (Co−NO)	$\Delta_f H°_{0K}$	$\Delta_f H°_{298K}$	$H°_{298K} - H°_{0K}$
$Co(CO)_3NO$			−405.7 ± 7	−406.0 ± 8	29.3
$Co(CO)_3NO^+$	91.7 ± 5[b]	126.1 ± 18	398.0 ± 9	401.5 ± 10	33.2
$Co(CO)_2NO^+$	111.1 ± 3[b]		603.5 ± 7	605.7 ± 8	26.4
$CoCONO^+$	151.0 ± 3[b]	157.7 ± 3[b]	828.5 ± 7	829.0 ± 7	19.3
$CoNO^+$		180.4 ± 7	1093.3 ± 7	1091.6 ± 7	11.8
$CoCO^+$	173.7 ± 6.8[c]		896.4 ± 7	898.1 ± 7	11.8
$Co(CO)_2^+$	152.4 ± 8.7[c]		630.1 ± 11		
$Co(CO)_3^+$	82.0 ± 12[c]		434.3 ± 16		
Co^+			1183.88 ± 1.0[d]		
CO			−113.81 ± 0.17[d]		
NO			89.775 ± 0.17[d]		

[a] In the $H°_{298K} - H°_{0K}$ calculations, the heat capacity of an electron was treated as 0.0 kJ/mol at all temperatures (the Rosenstock or ion convention[50]). To convert to the electron convention, 6.197 kJ/mol should be added to each 298 K ion heat of formation. For the derivation of the other quantities, see text. [b] From the present TPEPICO measurements. [c] From CID experiments of Armentrout.[29] [d] From the NIST-JANAF thermochemical tables.[49]

157.7 ± 3 kJ·mol^{-1} determined in the present TPEPICO experiment with the $\Delta_f H°_{0K}$ of NO (89.775 ± 0.17 kJ·mol^{-1}),[49] we derive a $CoCONO^+$ heat of formation of 828.5 ± 7 kJ·mol^{-1}. Finally, the other two $[Co(CO)_xNO-CO]^+$ dissociation energies ($x = 0$, 1) lead to zero Kelvin heats of formation of $Co(CO)_2NO^+$ at 603.5 ± 7 kJ·mol^{-1} and of $Co(CO)_3NO^+$ at 398.0 ± 9 kJ·mol^{-1}. The accuracy of the appearance energy determination in the present TPEPICO experiments is better than the accuracy of the adiabatic ionization energy determined from the TPES spectrum. Because of this, the heat of formation of the neutral $Co(CO)_3NO$ was directly determined from the heat of formation of $Co(CO)_2NO^+$ rather than from $Co(CO)_3NO^+$. The error bar given for this heat of formation, −405.7 ± 7 kJ·mol^{-1}, is actually lower than that of the molecular ion.

Other interesting thermochemical data can be extracted from the comparison of the present TPEPICO experiment with the CID results of Armentrout.[29] Cobalt nitrosyl dissociation energies can be calculated for the $[Co-NO^+]$ dissociation, as well as for $[Co(CO)_3-NO]^+$ dissociation. For the first one, we need $\Delta_f H°_{0K}[CoNO^+]$, which comes from the heat of formation of $CoCONO^+$, CO, and the $[CoNO-CO]^+$ dissociation energy determined in the TPEPICO experiments. This results in $\Delta_f H°_{0K}[CoNO^+] = 1093.3 \pm 7$ kJ·mol^{-1}. Using the previously listed heats of formation of the cobalt ion and nitrogen monoxide, the $[Co-NO]^+$ dissociation energy obtained is 180.4 ± 7 kJ·mol^{-1}. This number is in excellent agreement with the theoretical results of Thomas et al.,[48] which ranges from 163.3 to 178.0 kJ·mol^{-1} depending on the level of theory used.

The cobalt−nitrosyl dissociation energy in the molecular ion, $Co(CO)_3NO^+$ can also be calculated using the newly determined heat of formation of this ion along with the $Co(CO)_3^+$ heat of formation, $\Delta_f H°_{0K}[Co(CO)_3^+] = 434.3 \pm 16$ kJ·mol^{-1}, based on the successive Co−CO bond energy data (1.80 ± 0.07 eV, 1.58 ± 0.09 eV, and 0.85 ± 0.12 eV) reported by Goeble et al.[29] With these data, the cobalt-nitrosyl bond energy in $Co(CO)_3NO^+$ is found to be 126 ± 18 kJ·mol^{-1} or 1.31 ± 0.2 eV. As listed above, the first cobalt−carbonyl bond energy in $Co(CO)_3NO^+$ is significantly lower than this, 0.95 ± 0.02 eV. This is completely in line with the common findings that in transition metal organometallic complexes, the nitrosyl ligand is usually more strongly bound to the metal center than the carbonyl ligands, and also with our findings that in the TPEPICO experiments, no NO loss was observable from $Co(CO)_3NO^+$ or $Co(CO)_2NO^+$. Table 2 contains the thermochemical data derived above. Figure 6 shows the 0K thermochemistry of the $Co(CO)_3NO$ system. Solid arrows show dissociation energies (and the adiabatic IE) measured in the present TPEPICO measurements, while dashed arrows show quantities obtained from elsewhere.

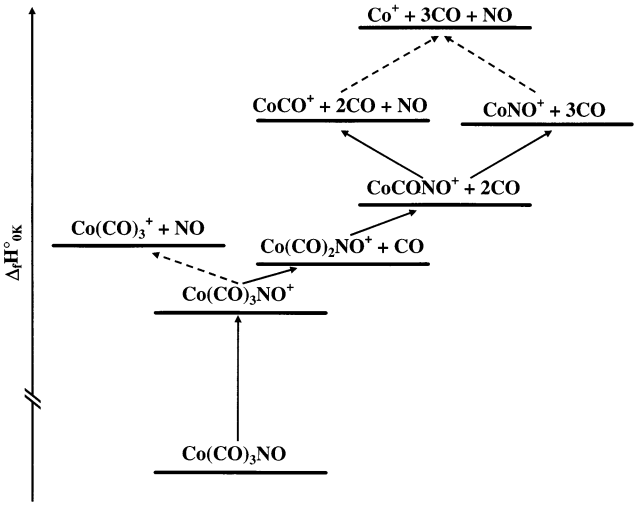

Figure 6. The 0 K thermochemistry of the $Co(CO)_3NO$ system. See text for details on the derivation of the heats of formation of the various species. Arrows pointing to the right indicate carbonyl loss, pointing to the left indicate nitrosyl loss. Solid arrows show dissociation energies (and the adiabatic IE) measured in the present TPEPICO measurements, while dashed arrows show quantities obtained from elsewhere.

To convert the above heat of formation data to room temperature, one has to calculate $H°_{298K} - H°_{0K}$ values for the $Co(CO)_3NO$ molecule and the various ions. We have done this using the scaled B3LYP/6-311G** frequencies. The $H°_{298K} - H°_{0K}$ values obtained are listed in Table 2. Using these data along with the $H°_{298K} - H°_{0K}$ values of the elements (Co, 4.771 kJ·mol^{-1}; C, 1.051 kJ·mol^{-1}; N_2, 8.670 kJ·mol^{-1}; and O_2, 8.683 kJ·mol^{-1}),[49] the following room temperature heat of formation data can be calculated: $\Delta_f H°_{298K}[Co(CO)_3NO] = -406.0 \pm 8$ kJ·mol^{-1}, $\Delta_f H°_{298K}[Co(CO)_3NO^+] = 401.5 \pm 10$ kJ·mol^{-1}, $\Delta_f H°_{298K}[Co(CO)_2NO^+] = 605.7 \pm 8$ kJ·mol^{-1}, $\Delta_f H°_{298K}[CoCONO^+] = 829.0 \pm 7$ kJ·mol^{-1}, $\Delta_f H°_{298K}[CoCO^+] = 898.1 \pm 7$ kJ·mol^{-1}, and $\Delta_f H°_{298K}[CoNO^+] = 1091.6 \pm 7$ kJ·mol^{-1}. Throughout these calculations the Rosenstock (or ion) convention was used, in which the heat capacity of an electron is treated as 0.0 kJ·mol^{-1} at all temperatures. One can convert the above values to the electron convention by adding 6.197 kJ·mol^{-1} to each ion 298 K heat of formation. All the derived heats of formation are listed in Table 2.

It is interesting at this point to revisit the calculated energy distributions shown in Figure 4. This calculation is for a total energy of 12.8 eV, which according to the breakdown diagram in Figure 2 lies at an energy at which 75% of the ions should be $CoCONO^+$, with the remaining ions consisting of a mixture of $CoCO^+$ and $CoNO^+$. It is clear from Figure 4 that all of the parent ions should be dissociated because the internal energy

is well above the $(CO)_2NOCo^+-CO$ bond energy of 0.95 eV. Similarly, the internal energy distribution of the $Co(CO)_2NO^+$ ion indicates that it should be fully dissociated. However, the $NOCo-CO^+$ and $COCo-NO^+$ bond energies of 1.565 and 1.63 eV, respectively, fall in the middle of the $CoCONO^+$ internal energy distribution. In fact, these bond energies are consistent with about 25% dissociation of the $CoCONO^+$ ion at the photon energy of 12.8 eV, just as observed in the breakdown diagram.

Conclusions

The sequential and in one case parallel dissociation paths of energy selected $Co(CO)_3NO^+$ ions have been investigated by threshold photoelectron photoion coincidence (TPEPICO) spectroscopy. The derivation of the 0 K bond dissociation energies required a careful modeling of the energy partitioning in the sequential dissociation steps. That is, while the parent ion can be energy selected with a narrow energy distribution, the fragment ions have much broader internal energy distributions that must be taken into account. This was accomplished by calculating the microcanonical energy partitioning using the statistical theory. This approach permitted fitting of the breakdown diagram up to the final products, $CoCO^+$ and $CoNO^+$, the limit of our photon energy. An interesting feature in the final dissociation step is the much looser transition state for NO loss than CO loss, which results in a rapid rise in the $CoCO^+$ signal relative to the $CoNO^+$ signal. Although, our photon source did not reach the energy required to break the last $Co-NO^+$ or $Co-CO^+$ bond, the latter bond energy is available from collision induced dissociation studies. As a result, it was possible to combine this bond energy with the TPEPICO measurements to obtain heats of formation of the neutral precursor, $Co(CO)_3NO$, its ion, as well as all the other ionic fragments. The energy scale was fixed to the well-known heat of formation of $Co^+ + 3CO + NO$. Using these heats of formation and published thermochemical data, other bond energies could be derived, which are in good agreement with expectations.

Acknowledgment. We thank the Hungarian Department of Education (grant number FKFP 0162/1999) and the U.S. Department of Energy for supporting this work. One of the authors (B.Sz.) thankfully acknowledges the generous support of the Magyari postdoctoral fellowship.

References and Notes

(1) Sztáray B.; Baer, T. *J. Am. Chem. Soc.* **2000**, *122*, 9219.
(2) Sztáray B.; Szepes, L.; Baer, T. *J. Am. Chem. Soc.* Submitted for publication.
(3) Li, Y.; Sztáray, B.; Baer, T. *J. Am. Chem. Soc.* **200**1, *123*, 9388.
(4) Li, Y.; McGrady, J. E.; Baer, T. *J. Am. Chem. Soc.* **2002**, *124*, 4487.
(5) Li, Y.; Sztáray, B.; Baer, T. *J. Am. Chem. Soc.* **2002**, *124*, 5843.
(6) Li, Y.; Baer, T. *J. Am. Chem. Soc.* **2002**, in press.
(7) Pályi, Gy.; Sampár Szerencsés, E.; Galamb, V.; Palágyi, J.; Markó, L. Hungarian patent HU 87-2105, 19870511, 1989.
(8) Roustan, J. L.; Bisnaire, M.; Park, G.; Guillaume, P. *J. Organomet. Chem.* **1988**, *356*, 195.
(9) Kubota, T.; Okamoto, H.; Okamoto, Y. *Jpn. Catal. Lett.* **2000**, *67*, 171.
(10) Mauge, F.; Vallet, A.; Bachelier, J.; Duchet, J. C.; Lavalley, J. C. *J. Catal.* **1996**, *162*, 88.
(11) Jiang, M.; Fu, Y. *Ranliao Huaxue Xuebao* **1998**, *26*, 75.
(12) Lene, P. A.; Oliver, P. E.; Wright, P. J.; Reeves, C. L.; Piit, A. D.; Cockayne, B. *Chem. Vap. Deposition* **1998**, *4*, 183.
(13) Ivanova, A. R.; Nuesca, G.; Chen, X.; Goldberg, C.; Kaloyeros, A. E.; Arkles, B.; Sullivan, J. J. *J. Electrochem. Soc.* **1999**, *146*, 2139.
(14) Smart, C. J.; Reynolds, S. K.; Stanis, C. L.; Patil, A.; Kirleis, J. T. *Mater. Res. Soc. Symp. Proc.* **1993**, *282*, 229.
(15) Londergan, A. R.; Nuesca, G.; Goldberg, C.; Peterson, G.; Kaloyeros, A. E.; Arkles, B.; Sullivan, J. J. *J. Electrochem. Soc.* **2001**, *148*, C21.
(16) West, G. A.; Beeson, K. W. U.S. Patent 4814294, 1989.
(17) Crawford, N. R. M.; Knutsen, J. S.; Yang, K.; Haugstad, G.; McKernan, S.; McCormick, F. B.; Gladfelter, W. L. *Chem. Vap. Deposition* **1998**, *4*, 181
(18) Hess, K. L.; Zehr, S. W. U.S. Patent 5045496, 1991.
(19) Hess, K. L.; Zher, S. W.; Cheng, W. H.; Pooladdej, J.; Buehring, K. D.; Wolf, D. L. *J. Cryst. Growth* **1988**, *93*, 576.
(20) Rana, R. K.; Koltypin, Y.; Gedanken, A *Chem. Phys. Lett.* **2001**, *344*, 256.
(21) Liu, S.; Zhu, J.; Mastai, Y.; Felner, I.; Gedanken, A. *Chem. Mater* **2000**, *12*, 2205.
(22) Liu, S.; Boeshore, S.; Fernandez, A.; Sayagues, M. J.; Fischer, J. E.; Gedanken, A. *J. Phys. Chem. B* **2001**, *105*, 7606.
(23) Foffani, A.; Pignataro, S.; Distefano, G.; Innorta, G. *J. Organomet. Chem.* **1967**, *7*, 473.
(24) Pignataro, S.; Lossing, F. P. *J. Organomet. Chem.* **1968**, *11*, 571.
(25) Lloyd, D. R.; Schlag, E. W. *Inorg. Chem.* **1969**, *8*, 2544.
(26) Hillier, I. H.; Guest, M. F.; Higginson B. R.; Lloyd, D. R. *Mol. Phys.* **1974**, *27*, 215.
(27) Baber, M.; Connor, J. A.; Guest, M. F.; Hall, M. B.; Hillier, I. H.; Meredith, W. N. E. *J. Chem. Soc., Faraday Discuss.* **1972**, *54*, 219.
(28) Chen, H. W.; Jolly, W. L. *Inorg. Chem.* **1979**, *18*, 2548.
(29) Goebel, S.; Haynes, C. L.; Khan, F. A.; Armentrout, P. B. *J. Am. Chem. Soc.* **1995**, *117*, 6994.
(30) Baer, T.; Booze, J. A.; Weitzel, K. M. Photoelectron Photoion Coincidence Studies of Ion Dissociation Dynamics. In *Vacuum Ultraviolet Photoionization and Photodissociation of Molecules and Clusters;* Ng, C. Y., Ed.; World Scientific: Singapore, 1991; p 259.
(31) Keister, J. W.; Baer, T.; Evans, M.; Ng, C. Y.; Hsu, C. W. *J. Phys. Chem.* **1997**, *101*, 1866.
(32) Becke, A. D. *J. Chem. Phys.* **1992**, *97*, 9173; Lee, C.; Yang, W.; Parr, R. G. *Phys. Rev.* **1988**, *B37*, 785.
(33) Krishnan, R.; Binkley, J. S.; Seeger, R.; Pople, J. A. *J. Chem. Phys.* **1980**, *72*, 650. Wachters, A. J. H. *J. Chem. Phys.* **1970**, *52*, 1033. Hay, P. J. *J. Chem. Phys.* **1977**, *66*, 4377.
(34) Pulay, P. *Mol. Phys.* **1969**, *17*, 197; reprint: *Mol. Phys.* **2002**, *100*, 57.
(35) Frisch, M. J.; Trucks, G. W.; Schlegel, H. B.; Scuseria, G. E.; Robb, M. A.; Cheeseman, J. R.; Zakrzewski, V. G.; Montgomery, J. A.; Stratmann, R. E.; Burant, J. C.; Dapprich, S.; Millam, J. M.; Daniels, A. D.; Kudin, K. N.; Strain, M. C.; Farkas, Ö.; Tomasi, J.; Barone, V.; Cossi, M.; Cammi, R.; Mennucci, B.; Pomelli, C.; Adamo, C.; Clifford, S.; Ochterski, J.; Petersson, G. A.; Ayala, P. Y.; Cui, Q, Morokuma, K.; Malick, D. K.; Rabuck, A. D.; Raghavachari, K.; Foresman, J. B.; Cioslowski, J.; Ortiz, J. V.; Baboul, A. G.; Stefanov, B. B.; Liu, G.; Liashenko, A.; Piskorz, P.; Komáromi, I.; Gomperts, R.; Martin, R. L.; Fox, D. J.; Keith, T.; Al-Laham, M. A.; Peng, C. Y.; Nanayakkara, A.; Gonzalez, C.; Challacombe, M.; Gill, P. M. W.; Johnson, B. G.; Chen, W.; Wong, M. W.; Andres, J. L.; Head-Gordon, M.; Replogle, E. S.; Pople, J. A. Gaussian 98, revision A.7; Gaussian, Inc.: Pittsburgh, PA, 1998.
(36) Chupka, W. A. *J. Chem. Phys.* **1959**, *30*, 191.
(37) Beyer, T.; Swinehart, D. R. *ACM Commun.* **1973**, *16*, 379.
(38) Baer, T.; Hase, W. L. *Unimolecular Reaction Dynamics: Theory and Experiments;* Oxford University Press: New York, 1996.
(39) Klots, C. E. *J. Chem. Phys.* **1973**, *58*, 5364.
(40) Kassel, L. S. *J. Phys. Chem.* **1928**, *32*, 225. Marcus, R. A.; Rice, O. K. *J. Phys. Colloid Chem.* **1951**, *55*, 894. Rice, O. K.; Ramsperger, H. C. *J. Am. Chem. Soc.* **1927**, *49*, 1617.
(41) Nelder, J. A.; Mead, R. *Comput. J.* **1965**, *7*, 308.
(42) Cox, J. D.; Pilcher, G. *Thermochemistry of Organic and Organometallic Compounds*; Academic Press: London, 1970.
(43) Rabinovich, I. B.; Nistratov, V. P.; Telnoy, V. I.; Sheiman, M. S. *Thermochemical and Thermodynamic Properties of Organometallic Compounds*; Begell House: New York, 1998.
(44) Linstrom, P. J.; Mallard, W. G. *NIST Chemistry WebBook*; NIST Standard Reference Database Number 69; National Institute of Standards and Technology: Gaithersburg, MD, 2001.
(45) Hanratty, M. A.; Beauchamp, J. L.; Illies, A. J. van Koppen, P. A. M.; Bowers, M. T. *J. Am. Chem. Soc.* **1988**, *110*, 1.
(46) Carpenter, C. J.; van Koppen, P. A. M.; Bowers, M. T. *J. Am. Chem. Soc.* **1995**, *117*, 10976.
(47) Barnes, L. A.; Rosi, M.; Bauschlicher, Jr., C. W. *J. Chem. Phys.* **1990**, *93*, 609.
(48) Thomas, J. L. C.; Bauschlicher, Jr., C. W.; Hall, M. B. *J. Phys. Chem.* **1997**, *101*, 8530.
(49) Chase, M. W. NIST-JANAF Thermochemical Tables. *J. Phys. Chem. Ref. Data, Monogr. 9* **1998**.
(50) Rosenstock, H. M.; Draxl, K.; Steiner, B. W.; Herron, J. T. *Energetics of Gaseous Ions; Journal of Physical Chem. Reference Data Vol. 6*; American Chemical Society: Washington, DC, 1997.